2021

Simulating Systematic Errors in Exoplanetary Transits for the James Webb Space Telescope

David C. Wright III
University of Central Florida

SIMULATING SYSTEMATIC ERRORS IN EXOPLANETARY TRANSITS FOR THE JAMES WEBB SPACE TELESCOPE

by

DAVID C. WRIGHT III

A thesis submitted in partial fulfillment of the requirements
for the Honors in the Major Program in Physics
in the College of Sciences
and in the Burnett Honors College
at the University of Central Florida
Orlando, Florida

Spring Term
2021

Thesis Chair: Joseph Harrington

ABSTRACT

The James Webb Space Telescope (JWST) is a next-generation space telescope that will be capable of making transformative observations of planetary transits. As its launch date grows ever closer, it becomes imperative that astronomers have access to accurate simulations of JWST observations in order to best plan observations and devise data analysis pipelines. Unfortunately, available simulation tools do not provide the most accurate or realistic simulations, including noise and systematic errors. In this thesis, I present an open-source time-domain simulator of planetary transits that is capable of accurately modeling these effects in observations made by JWST.

TABLE OF CONTENTS

LIST OF FIGURES

LIST OF TABLES

CHAPTER 1: INTRODUCTION

Exoplanet transit observations yield information on the target planet's atmospheric properties. This technique has so far only been used to study a small fraction of the more than 4,000 discovered exoplanets. The upcoming James Webb Space Telescope (JWST) offers multiple observation modes tailored specifically for exoplanet transit observations (Beichman *et al.* 2014). With numerous targets to observe and cutting edge instrumentation, JWST is poised to propel exoplanet science to new heights.

Simulation tools for JWST exoplanet transit observations are needed in order to prepare data reduction pipelines and properly constrain the errors on observations. Due to the time-domain nature of transit observations, accurate models of time-correlated noise, such as instrument jitter, are required. Ideally, a simulation tool would be able to create data that is as close as possible to real observation data. The current simulation tools available for JWST do not satisfy these requirements.

In this thesis, I present an open-source JWST simulation tool that creates accurate, time-series data, including instrument systematics and noise akin to a real observation. Starting with ExoSim (Sarkar *et al.* 2020b, 2016) as the code base, I develop the required features to simulate JWST and integrate them into a fork of ExoSim. I then validate the code to ensure it produces accurate simulations, simulate the instruments and modes most useful for exoplanet science, and compare these simulations with simulations from other tools.

CHAPTER 2: LITERATURE REVIEW

Planetary Transits

Mayor and Queloz (1995) discovered the first exoplanet orbiting a sun-like star. The planet, dubbed 51 Pegasi b, was detected via periodic variations in its host star's radial velocity (for an overview of this method, see Lovis and Fischer 2010 and Mayor *et al.* 2014). Soon after, in December of 1999, a planet (HD 209458 b) was discovered via photometric observations of it transiting its star for the first time (Charbonneau *et al.* 2000). During a transit, the fractional decrease in flux (Figure 2.1) as the planet passes in front of its star is approximately equal to $(R_p/R_*)^2$, where R_p and R_* are the radius of the planet and star, respectively. This quantity is found by fitting model light curves (Mandel and Agol 2002) to the transit data. It is a small ratio, around 1-2% for a typical hot Jupiter. From the transit timings and stellar mass, the mass of the planet can be estimated. The radius found in transit allows for calculations of quantities such as the surface gravity and average density. In 2002, Charbonneau *et al.* (2002) followed up with a spectroscopic observation of another HD 209458 b transit that confirmed predictions Seager and Sasselov (2000) had made about the planet's atmosphere.

Now, over two decades since the discovery of the first exoplanet, more than 4000 have been detected. Spectroscopic observations of transits and eclipses, when the planet passes in front of and behind its host star (Seager and Sasselov 2000, Charbonneau *et al.* 2002, Seager and Deming 2010, Crossfield 2015, Madhusudhan 2019), have been the most successful methods for characterizing exoplanet atmospheres. The observed spectra carry information about the atmosphere's chemical and physical processes, from which astronomers can get a glimpse at the planet's atmospheric processes and the history of formation and evolution.

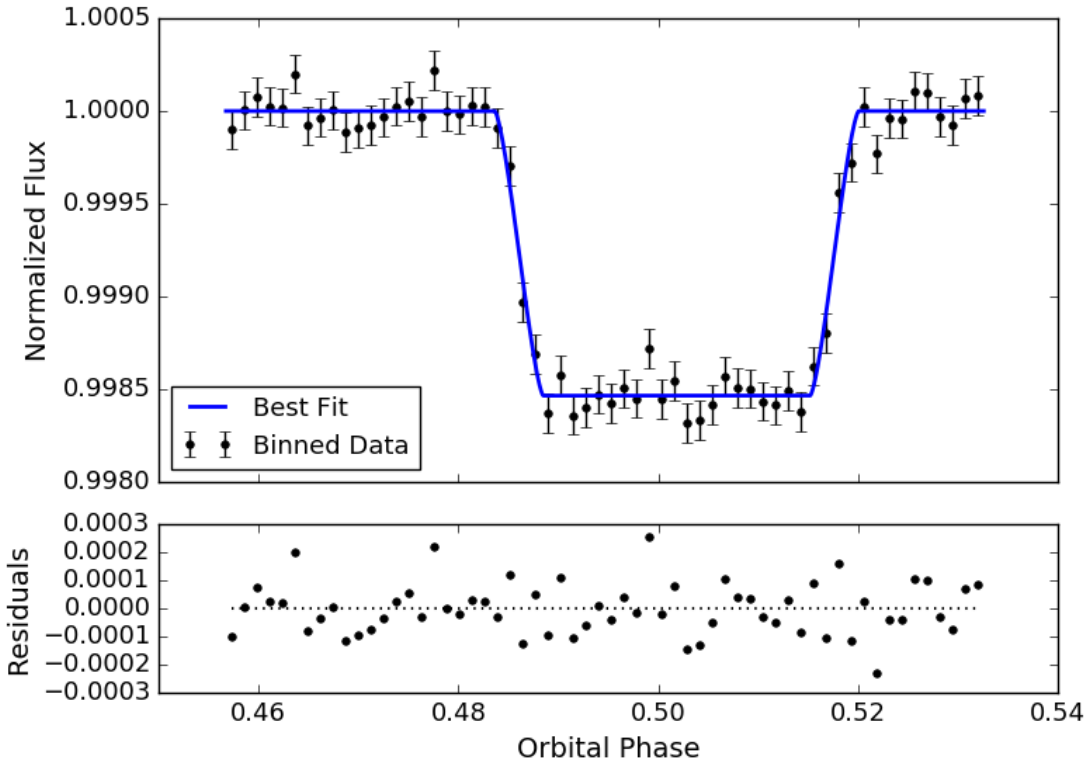

Figure 2.1: A light curve fit to HD 209458 b transit data.

The James Webb Space Telescope

Over the decades, the two most prominent telescopes that have been used for exoplanet discovery and characterization are the Hubble and Spitzer Space Telescopes (Deming *et al.* 2005, 2013, Harrington *et al.* 2006, Mazeh *et al.* 2000, Sing *et al.* 2011, Beichman and Deming 2017). At launch, neither had exoplanet science in their mission plans. JWST was built before exoplanets became a major focus, but was calibrated with exoplanet science in mind (Stevenson *et al.* 2016, Greene *et al.* 2016).

Webb carries four instruments on board: the Near-InfraRed Camera (NIRCam, Beichman *et al.*

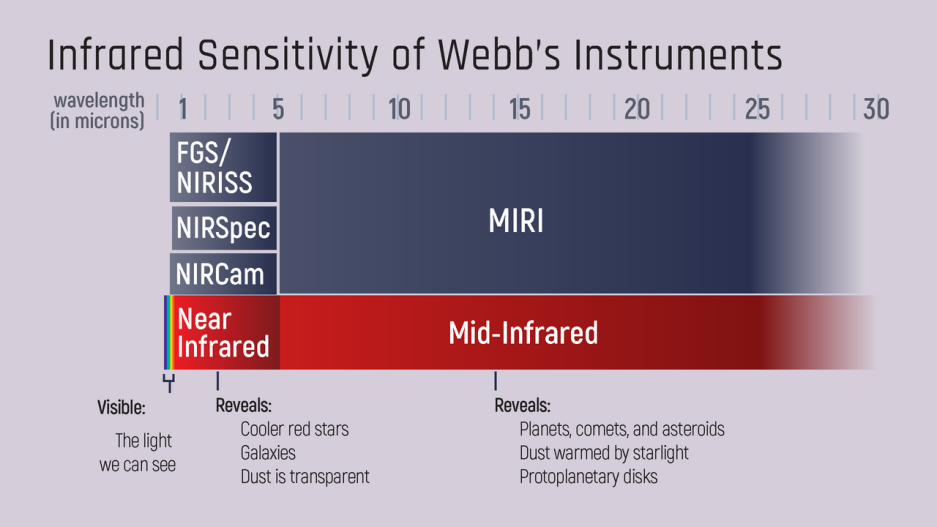

Figure 2.2: Overview of JWST's instruments wavelength coverage. Image credit: STScI.

2012, the Near-InfraRed Spectrograph (NIRSpec, Ferruit *et al.* 2012), the Near Infrared Imager and Slitless Spectrograph (NIRISS, Doyon *et al.* 2012), and the Mid-Infrared Instrument (MIRI, Kendrew *et al.* 2015, Rieke *et al.* 2015, Wells *et al.* 2015). Each of these instruments can be utilized in exoplanet transit studies. Its primary mirror, measuring $25m^2$, is the largest of any space telescope yet. Orbiting around the Earth-Sun L2 point, JWST will make stable observations over long periods of time. Webb is extremely sensitive when compared to other missions over its $0.6 - 28$ μm range (see Figure 2.2), and its detectors are capable of much better than 100 parts per million (ppm) precision over time periods from hours to days (Beichman *et al.* 2014). All this combined makes JWST an excellent observatory for exoplanet science.

Simulating JWST

A number of simulators have already been developed, both specific to single instruments and generalized to all instruments. Batalha *et al.* (2015) presented a NIRSpec simulator that includes

shot noise, read noise, jitter, and convolution with the point-spread function (PSF) and intrapixel-response function. It is written in IDL and is not open-source, two characteristics which negatively impact its adoption. This code's ability to model time-dependent effects is also not well documented. Louie *et al.* (2018) reported a NIRISS Single Object Slitless Spectroscopy (SOSS) simulator which mainly focuses on estimating signal to noise ratios (S/N) and not on realistic simulated images. For example, it does not model the 2D curved spectral trace of NIRISS SOSS nor the multiple orders of NIRISS SOSS. PyNRC[1], an open-source NIRCam simulator written in Python, aims to reproduce realistic JWST images and spectra.

As for more generalized simulators, PandExo (Batalha *et al.* 2017) was recently developed to simulate all instruments and modes with an accessible interface. It makes use of the Pandeia engine (Pontoppidan *et al.* 2016), which is also used in Webb's Exposure Time Calculator (ETC). While Pandeia's stated goal is to provide S/N estimates for observables, PandExo aims to provide observation simulations of each timeseries spectroscopy mode. Both PandExo and Pandeia are open-source Python codes. While PandExo is great as a first estimate of performance for a given observation, it does not simulate all effects and potential sources of noise, such as jitter noise.

All of the previously mentioned simulators are static: they do not directly model the time domain. JexoSim (Sarkar *et al.* 2020a) aims to differentiate itself from the other tools by doing this. Based on ExoSim (Sarkar *et al.* 2020b), JexoSim "generates signal and noise using a dynamical approach" and can model complex, time-dependent effects. Unlike ExoSim, however, JexoSim is not an open-source code. JexoSim also lacks the ability to model multiple-order spectra and emulate all of Webb's detector readout patterns.

[1] https://github.com/JarronL/pynrc

CHAPTER 3: METHODOLOGY

Overview of ExoSim

ExoSim is a modular, time-domain simulator of exoplanet transits (Sarkar *et al.* 2020b). ExoSim simulates the full light curve, including instrument noise and systematic errors. An ExoSim simulation is configured using a user-supplied XML file containing the parameters for the instrument(s) and observation. Users can specify parameters such as which noise sources to include, whether to simulate a transit or eclipse, and the planet to observe.

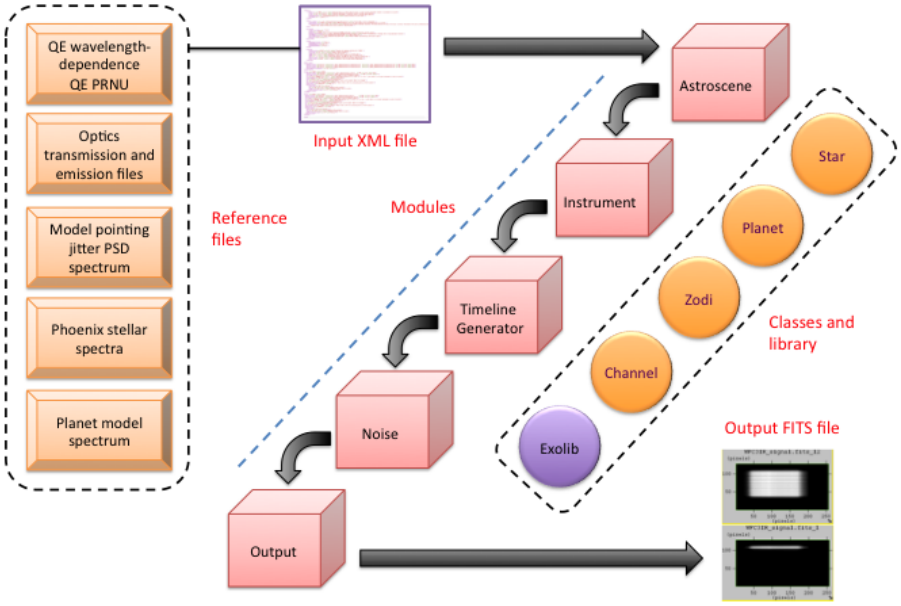

Figure 3.1: Overview of ExoSim algorithm. Image Credit: Enzo Pascale

Astroscene

After reading in the XML configuration file, the ExoSim algorithm (Figure 3.1) moves on to the *Astroscene* module. In this module, the *Star* and *Planet* object classes are instantiated using a PHOENIX stellar model (Allard *et al.* 2012) and the Open Exoplanet Catalogue (Rein 2012), respectively. The flux density at the telescope aperture is calculated in *Astroscene* as

$$F_{Tel}(\lambda) = F_S(\lambda)\left(\frac{R_S}{D}\right)^2, \tag{3.1}$$

where $F_S(\lambda)$ is the star's surface flux density, R_S is the star's radius, and D is the distance from the telescope to the star. Wavelength-dependent light curves are generated by the *Planet* class using the methods presented by Mandel and Agol (2002). Zodiacal light is also modeled using the *Zodi* object class.

Instrument

In the *Instrument* module, the incoming flux is modulated by the optical elements of the telescope. The power per unit wavelength at the telescope is given by

$$P_{Tel}(\lambda) = A_{Tel}F_{Tel}(\lambda), \tag{3.2}$$

where A_{Tel} is the area of the telescope's aperture. The throughput of each optical element in the common optics is given in the XML configuration file by pointing to a reference file with the requisite information. ExoSim combines the throughput of each common optical element to arrive at a net throughput, $\eta_{Tel}(\lambda)$. The power per unit wavelength after passing through the common

optics is then

$$P_{Com}(\lambda) = P_{Tel}(\lambda)\eta_{Tel}(\lambda). \tag{3.3}$$

After passing through the common optics, the light is then modulated by one or more instruments. Each instrument is instantiated as a *Channel* object class in ExoSim. ExoSim supports both spectrometer and photometer instruments. The *Channel* object contains the optical surfaces, dispersion relation, detector parameters, and other specifics for each instrument channel. A net throughput, $\eta_{Ch}(\lambda)$, is calculated for each instrument channel. The power per unit wavelength that will reach the detector is then

$$P_{Det}(\lambda) = P_{Com}(\lambda)\eta_{Ch}(\lambda). \tag{3.4}$$

Before the light falls on the detector, it is convolved with a wavelength-dependent point-spread function (PSF). At this point, the detector is oversampled such that each PSF is Nyquist sampled. The PSF images are placed on the detector according to the dispersion relation, $\lambda(x)$, given in the configuration file. To simulate a photometer, the PSF images in the photometer's wavelength range are coadded over the same location on the detector. By default, ExoSim assumes that the each PSF lies directly in the center of the detector in the y direction. The volume of each PSF is equal to the power incident on the pixel column.

Each pixel on the detector now has power $P_{Pix}(x,y)$. Using the quantum efficiency provided in the

configuration file, the number of electrons per second produced in each pixel can be calculated as

$$Q(x,y) = P_{Pix}(x,y)QE(x,y)\frac{hc}{\lambda(x)} \tag{3.5}$$

The thermal emission from the instrument and the zodiacal light are also added during this stage. An intra-pixel response function which models the fall in responsivity towards the edges of a pixel is convolved with the oversampled detector array. The detector is then downsampled back to single pixel resolution.

Timeline

The *Timeline* module sets up the series of exposures contained within a observation. Each exposure consists of a number of non-destructive reads (NDRs) and a detector reset. The frame rate, reset time, and 'dead time' between a NDR and reset can be specified in the configuration file. The detector array generated in the *Instrument* module is used to generate a 3D data-cube of NDRs over time. Given the integration time for each NDR, the number of electrons generated per pixel can now be calculated. For computational efficiency, the transit light curve is not applied in the *Timeline* module, but in the *Noise* module.

Noise

In the noise module, both uncorrelated and correlated noise sources are added to the detector signal. Uncorrelated noise sources include photon noise, thermal emissions from the detector, and detector read noise. The individual pixel counts are randomly adjusted to simulate the effects of these noise sources. The main source of correlated noise that is modeled by ExoSim is pointing

jitter. A jitter power spectral density (PSD) is supplied in the configuration file. ExoSim uses the PSD to generate slight shifts of the x and y positions of the detector over small timescales within each integration. Each of these small timescale simulations within an integration is coadded to result in a final integration.

Output

ExoSim outputs FITS files, much like a real observation. The FITS headers include information on the simulation, such as the target planet and wavelength solution $\lambda(x)$ of the detector. No post-processing is done on the images, so the output of the simulation is very close to the raw output of an instrument.

Development

Curved Spectral Traces

The Single Object Slitless Spectroscopy (SOSS) mode of the NIRISS instrument (Figure 3.2) was specifically designed for transit spectroscopy. It uses the GR700XD crossed-dispersed grism to produce a multiple-ordered, curved spectral trace on the detector. However, ExoSim was originally designed to simulate only flat spectral traces. In order to simulate curved traces, I modified ExoSim to allow a 2D wavelength solution $\lambda(x,y)$. All aspects of ExoSim which were built for only flat spectral traces, such as the generation of light curves, were modified to allow for curved cases. The user can now supply a 2D wavelength solution in the configuration file.

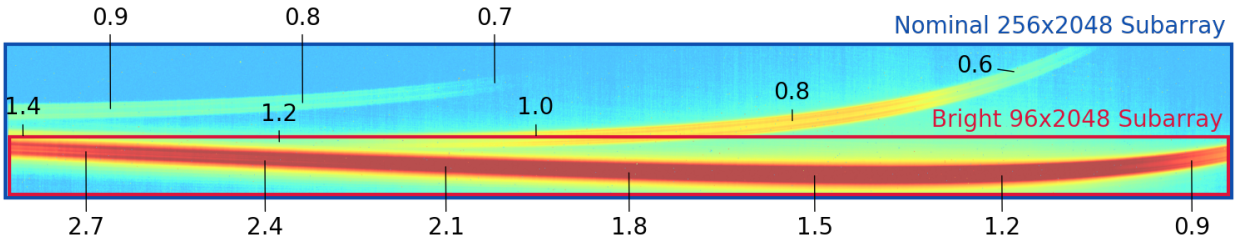

Figure 3.2: NIRISS SOSS. Three orders cover a wavelength range of 0.6 µm–2.8 µm. Image Credit: STScI

Multiple-ordered Spectra

ExoSim was not designed to simulate multiple-ordered spectral traces. As seen in Figure 3.2, NIRISS SOSS creates three orders of cross-dispersed spectra. Many aspects of ExoSim rely on interpolation of wavelength dependent values; however, with multiple ordered traces, it is possible for the different orders' wavelength ranges to overlap. The solution to this issue is to create separate grids for each order. Effectively, a separate detector is simulated for each order and then later coadded to give the original detector image, taking care not to double count or incorrectly modify any noise effects. Also, order dependent throughput calculations were added to the *Instrument* module of ExoSim.

Detector Read-out Patterns

The basic unit of a JWST readout pattern is a *frame*. A *group* consists of a series of non-destructively read frames and possibly skipped frames at the end of the group that are not saved. The frames in a group are averaged by the on-board electronics. A destructive read followed by collection of groups is an *integration*. An *exposure* is a set of integrations. See Table 3.1 for example readout patterns.

In ExoSim, the *group* found in the JWST readout scheme (Figure 3.3) does not exist. I added the

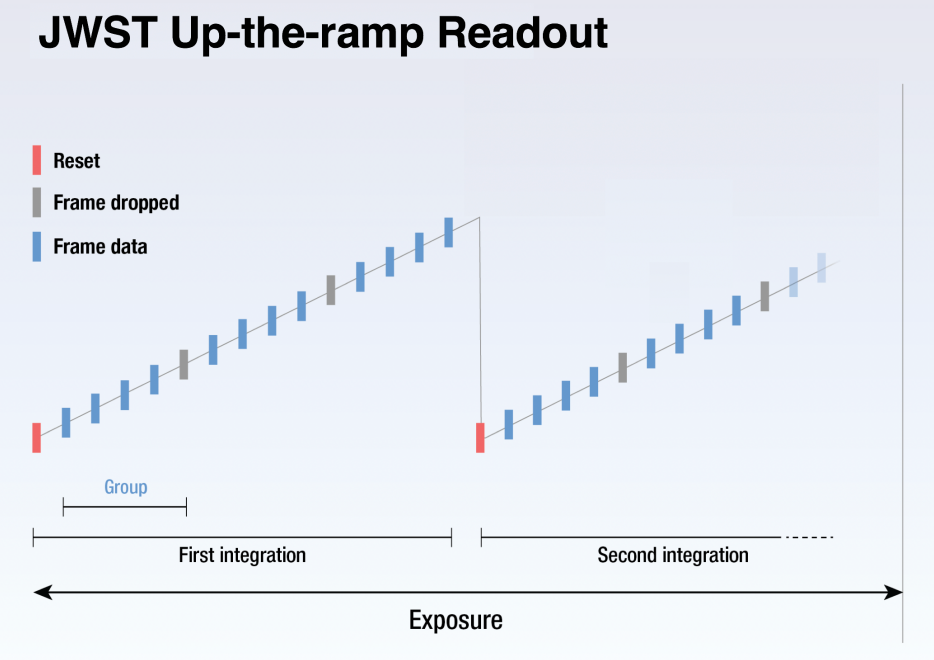

Figure 3.3: General structure of detector readout scheme used by all JWST Near-IR detectors. Image Credit: STScI

Readout Pattern	N_{frames}	N_{skip}
NISRAPID	1	0
NIS	4	0
NRSRAPIDD1	2	1
SHALLOW4	5	1

Table 3.1: Example JWST readout patterns.

option to specify a JWST readout scheme in the configuration file, and I added a new function to average the frames as needed, while also making sure to include all noise sources.

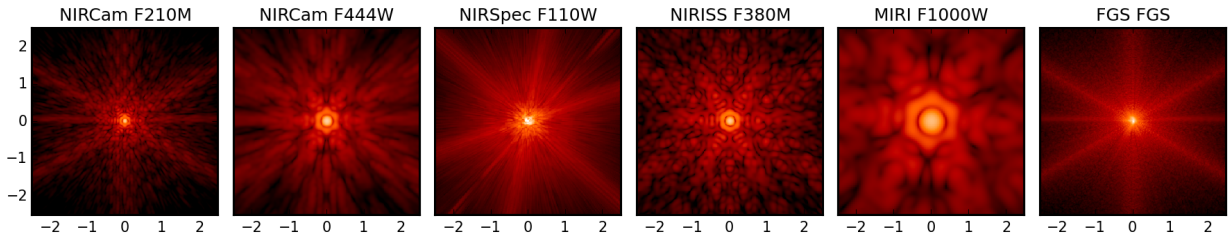

Figure 3.4: Sample PSFs for JWST's instrument suite, all on the same angular scale and display stretch. Image Credit: STScI.

WebbPSF

A collection of monochromatic PSFs produced by WebbPSF (Perrin *et al.* 2014) is available for each instrument configuration in the reference data provided by Pandeia (Pontoppidan *et al.* 2016). ExoSim is capable of using 3rd-party PSFs, but it required modifications to read the FITS files that WebbPSF creates. I wrote new functions to read in WebbPSF FITS files and also a parallelized routine to generate new PSFs using WebbPSF over a given wavelength grid.

Parallelization

JWST detector subarrays can be extremely large. Take for instance NIRISS SOSS. Its SUBSTRIP256 subarray is 256x2048 pixels. With these large detectors and the changes that were made to accommodate multiple-ordered spectra, ExoSim very often came to a crawl when running simulations. I noticed some sections of ExoSim that lent themselves to parallelization, and used Dask to run those sections of the code in parallel. Dask[1] is "flexible library for parallel computing in Python" that's designed to be a drop-in replacement for the NumPy and Pandas libraries. Dask builds a task graph (Figure 3.5) over time, and evaluates the tasks in the graph by efficiently as-

[1] https://dask.org/

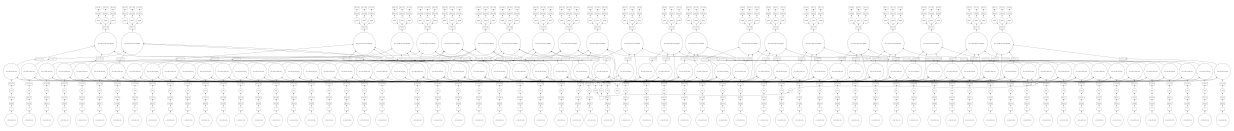

Figure 3.5: Visual representation of a Dask task graph built during ExoSim execution.

signing them to the resources the user has provided only when the final result of the tasks in the graph are requested. Users can specify how many processors and how much memory they would like to give an ExoSim simulation.

Validation

Focal Plane Signal

A simulation without noise was performed for an out-of-transit observation of the star 55 Cancri. The star was modeled as a black body with an effective temperature of 5172 K. In this test, the PSFs were represented as a series of delta functions, i.e., all of the signal fell directly on individual pixels. The focal plane was saved to disk in the *Instrument* module. The columns of the focal plane were summed over, and the resulting signal was compared to the predicted value given by

$$Q(x) = \pi B_{\lambda(x)}(5192\,\mathrm{K})\left(\frac{R_S}{D}\right)^2 A_{Tel}\eta_{Ch}(\lambda(x))QE(x)\Delta\lambda(x)\frac{\lambda(x)}{hc}. \tag{3.6}$$

In order to validate the implementation of multiple order traces, a noiseless simulation of two orders was performed separately and together for a total of three images. The out-of-transit, black body system described previously was used in these simulations. The two individual simulated images were summed and compared to the simulation of the orders on the same detector.

Comparison to Original ExoSim

Sarkar *et al.* (2020b) extensively validated each noise source. I have not directly modified any of the noise models in ExoSim. In order to show that my changes have not impacted these models in any way, I ran simulations in my modified version of ExoSim and in the original version of ExoSim using the same configuration file and reference data. I first ran a simulation without noise, and then another simulation for each noise source with *only* that noise source enabled. For each of these simulations, I used the fitsdiff[2] utility to compare the fits files produced.

Comparison to PandExo

JexoSim (Sarkar *et al.* 2020a) and PandExo (Batalha *et al.* 2017) are the two tools mentioned which are comparable to my modified version of ExoSim. However, JexoSim is not publicly available, so comparisons between simulations are only possible with PandExo. Simulations of all four instruments configured for exoplanet transit observations were compared. In these simulations, all noise sources were disabled except for shot noise. NIRSpec was set to observe 55 Cancri out-of-transit, and the star was modeled as a black body. The next instrument to be compared was NIRISS in its SOSS mode. 55 Cancri proved to be too bright of a target for NIRISS SOSS, so GJ 1214 was used instead. This observation was also out of transit, and the star was modeled as a black body. The same observation scene was used for MIRI in its low-resolution spectroscopy (LRS) mode and NIRCam in its grism time-series mode. See Table 3.2 for an overview of the instrument configurations.

Both PandExo and ExoSim simulations were processed using the first-minus-last strategy (correlated double sampling or CDS) to get the flux incident on the detector. The resulting flux measure-

[2]http://stsdas.stsci.edu/stsci_python_epydoc/pytools/fitsdiff.html

ments are binned to a common wavelength grid using PandExo's binning tools.

	NIRSpec BOTS	NIRCam	NIRISS SOSS	MIRI LRS
Subarray	SUB512	SUBGRISM64	SUBSTRIP256	SLITLESSPRISM
Size	32×512	64×2048	256×2048	72×416
W_{slit} (pix)	16	N/A	N/A	N/A
Δ_{pix}(μm)	18	18	18	25
PS($^\circ \times 10^{-5}/\Delta_{pix}$)	2.78	1.75	1.81	3.06
T(K)	40	40	40	7

Table 3.2: Configuration parameters for the PandExo and ExoSim comparison simulations. W_{slit} is the slit width in pixels, Δ_{pix} is the size of a pixel in microns, PS is the plate scale in degrees per pixel, and T is the instrument temperature in Kelvin. Only the 1st order of NIRISS SOSS was simulated because PandExo cannot simulate multiple orders.

CHAPTER 4: RESULTS

Capabilities

JWST Instrument Simulations

ExoSim is now capable of simulating all instruments and modes on JWST. Figure 4.1 utilizes all of the features which have been built into the modified version of ExoSim in order to model JWST instruments, i.e., curved spectral traces, multiple-ordered spectral traces, instrument specific PSFs, and instrument specific readout patterns.

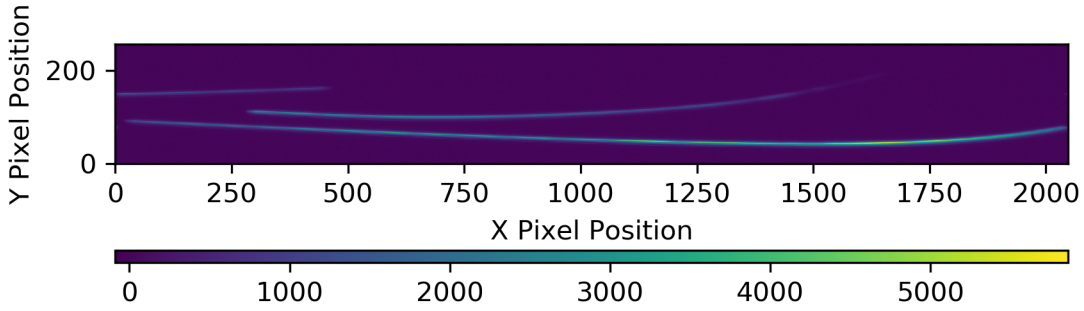

Figure 4.1: NIRISS SOSS ExoSim simulation. WebbPSF PSFs were used along with the NISRAPID readout pattern.

Parallelization

By using 20 processors in parallel, I was able to decrease the run-time of an intensive simulation from over two hours to just eight minutes. This relationship is almost exactly inversely proportional, but there are some sections of the code which cannot be parallelized. Also, the Dask library

allows for distributed computing on standard university computing clusters. By changing a single option in the code, users can run ExoSim on their university computing clusters with possibly hundreds of processors.

Validation

Focal Plane Signal

The results of the focal plane validation tests are shown in Figure 4.2. The simulation matches the prediction almost exactly. What little error is present is most likely due to interpolation error because the black body prediction is calculated at each wavelength of interest, but the simulated black body SED is interpolated over the wavelength grid.

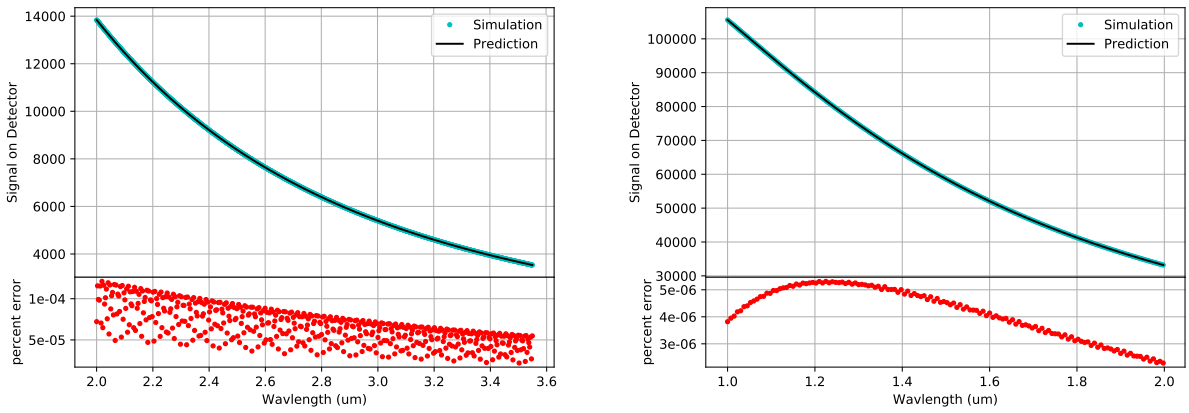

(a) Flat spectral trace

(b) Curved spectral trace

Figure 4.2: Comparison of predicted black body signal to simulation.

The validation test of the multiple-ordered spectral traces using fitsdiff resulted in fits files which were exactly the same, showing that the method is valid.

Comparison to Original ExoSim

For each simulation pair consisting of an original ExoSim simulation and a modified ExoSim simulation, fitsdiff reported no differences between the FITS files for each simulation. This shows that each noise model has remained unmodified by my changes elsewhere in ExoSim, and the original validation of these models holds.

Comparison to PandExo

The results of the simulations are shown in Figure 4.3. Out of all the instruments, NIRSpec showed the best agreement with PandExo. ExoSim has an average percent difference from PandExo of $+1.53 \pm 1.63\%$. JexoSim (Sarkar *et al.* 2020a) is also based on ExoSim but reported an average percent difference with PandExo of $+15.8 \pm 5.6\%$. NIRCam follows after NIRSpec with an average percent difference of $+2.18 \pm 1.08\%$. JexoSim reports an average percent difference of $+3.0 \pm 2.2\%$. The ExoSim MIRI simulation has an average percent difference from the PandExo simulation of $+3.61 \pm 2.63\%$. The corresponding JexoSim simulation has an average percent difference from PandExo of $-1.0 \pm 4.0\%$. The instrument that exhibited the worst comparison was NIRISS. The NIRISS SOSS ExoSim simulation had an average percent difference with the corresponding PandExo simulation of $+4.54 \pm 1.37\%$. JexoSim also reports a similiar percent difference at $+4.1 \pm 2.4\%$

Overall, the modified version of ExoSim produces simulations which are adequately similar to PandExo. Given that the validation tests were extremely successful, the cause of the differences between ExoSim and PandExo is most likely the different internal models of the instruments and not a flaw with ExoSim. PandExo is a radiometric simulator that is meant primarily for providing accurate S/N estimates. ExoSim, however, is focused around digitizing the focal plane and gener-

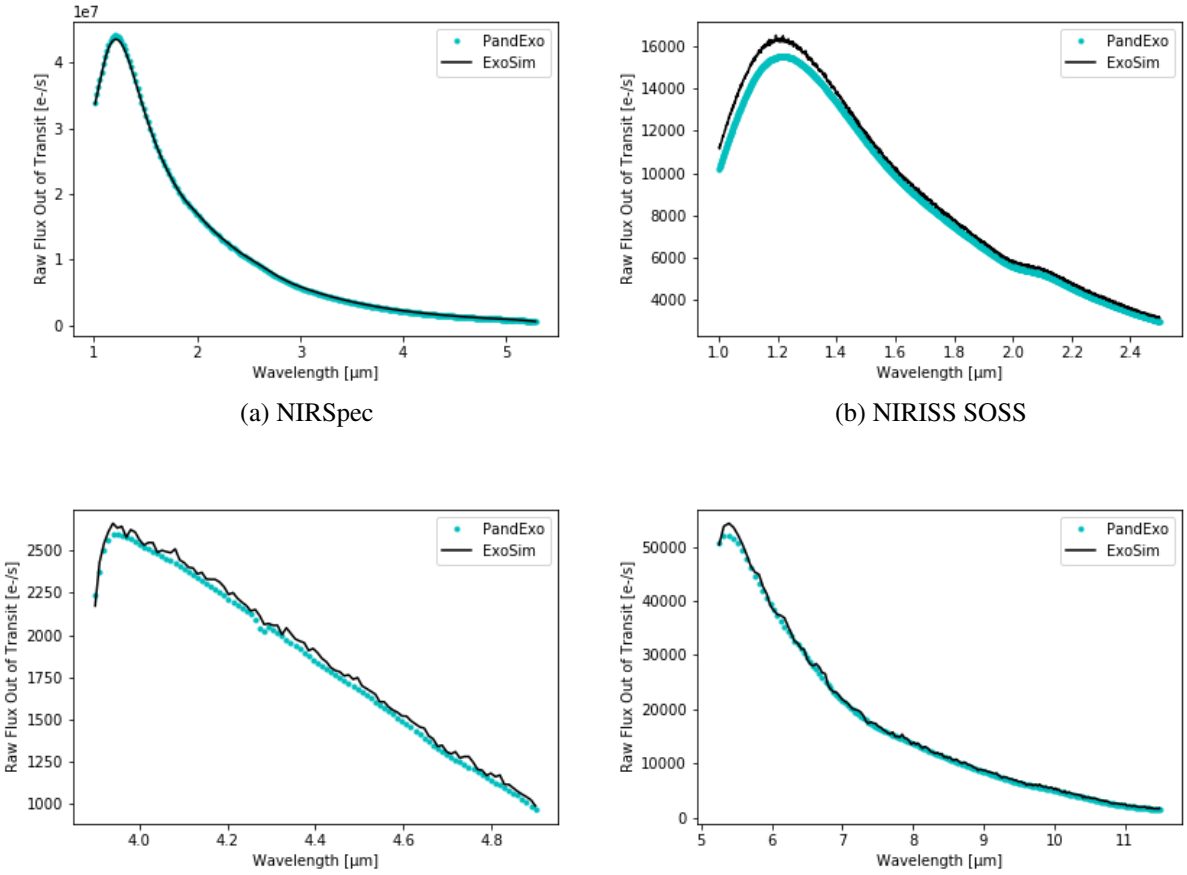

(a) NIRSpec

(b) NIRISS SOSS

(c) NIRCam Grism-R/F444W

(d) MIRI LRS

Figure 4.3: Comparison of ExoSim and PandExo simulations.

ating realistic time-domain data. Finding the specific cause of the differences requires an in-depth study of PandExo and Pandeia which is outside the scope of this thesis. This will be part of future work.

CHAPTER 5: CONCLUSION

Future Work

Two of the most time consuming tasks when working with ExoSim are sourcing reference files and configuring the instruments. It would be beneficial to write code to bridge ExoSim and the Pandeia reference data directly. Users would be able to simply specify the name of the filter, disperser, etc. and ExoSim would find and use the correct reference data.

An in depth study of PandExo and Pandeia is needed to find the cause of the differences observed in this thesis. This study could also be done in tandem with the previous future work mentioned.

Outside of future work to be done to ExoSim, using ExoSim to simulate known exoplanet spectra and then running atmospheric retrieval code on the simulated spectra is an interesting prospect. This end-to-end simulation and retrieval would allow astronomers to benchmark the performance of instruments in regards to specific exoplanet observations or specific observational goals, such as detecting water vapor in an exoplanet's atmosphere.

Closing Remarks

In this thesis, I described the development and validation of a time-domain simulator of exoplanet transits and systematic errors based on ExoSim (Sarkar *et al.* 2020b). The simulator produces a sequence of FITS files in the time domain, much like a real observation. This modified version of ExoSim is open-source and available to the community with the hope that it will be used to further our understanding of the effects of systematic noise on exoplanet transits and to prepare for observations of exoplanet transits with the James Webb Space Telescope.

LIST OF REFERENCES

Allard, F., D. Homeier, and B. Freytag, Models of very-low-mass stars, brown dwarfs and exoplanets, *Philosophical Transactions of the Royal Society A: Mathematical, Physical and Engineering Sciences* **370**, 1968, 2765–2777, 2012. Publisher: Royal Society.

Batalha, N., J. Kalirai, J. Lunine, M. Clampin, and D. Lindler, Transiting Exoplanet Simulations with the James Webb Space Telescope, *arXiv:1507.02655 [astro-ph]* , 2015. ArXiv: 1507.02655.

Batalha, N. E., A. Mandell, K. Pontoppidan, K. B. Stevenson, N. K. Lewis, J. Kalirai, N. Earl, T. Greene, L. Albert, and L. D. Nielsen, PandExo: A Community Tool for Transiting Exoplanet Science withJWST&HST, *Publications of the Astronomical Society of the Pacific* **129**, 976, 064,501, 2017. Publisher: IOP Publishing.

Beichman, C., B. Benneke, H. Knutson, R. Smith, P.-O. Lagage, C. Dressing, D. Latham, J. Lunine, S. Birkmann, P. Ferruit, G. Giardino, E. Kempton, S. Carey, J. Krick, P. D. Deroo, A. Mandell, M. E. Ressler, A. Shporer, M. Swain, G. Vasisht, G. Ricker, J. Bouwman, I. Crossfield, T. Greene, S. Howell, J. Christiansen, D. Ciardi, M. Clampin, M. Greenhouse, A. Sozzetti, P. Goudfrooij, D. Hines, T. Keyes, J. Lee, P. McCullough, M. Robberto, J. Stansberry, J. Valenti, M. Rieke, G. Rieke, J. Fortney, J. Bean, L. Kreidberg, D. Ehrenreich, D. Deming, L. Albert, R. Doyon, and D. Sing, Observations of Transiting Exoplanets with the James Webb Space Telescope (JWST), *Publications of the Astronomical Society of the Pacific* **126**, 946, 1134, 2014. Publisher: IOP Publishing.

Beichman, C. A. and D. Deming, Observing Exoplanets with the Spitzer Space Telescope, in *Handbook of Exoplanets*, H. J. Deeg and J. A. Belmonte, eds., pp. 1–25, Springer International Publishing, Cham, 2017.

Beichman, C. A., M. Rieke, D. Eisenstein, T. P. Greene, J. Krist, D. McCarthy, M. Meyer, and J. Stansberry, Science opportunities with the near-IR camera (NIRCam) on the James Webb Space Telescope (JWST), in *Space Telescopes and Instrumentation 2012: Optical, Infrared, and Millimeter Wave*, vol. 8442, p. 84422N, International Society for Optics and Photonics, 2012.

Charbonneau, D., T. M. Brown, D. W. Latham, and M. Mayor, Detection of Planetary Transits Across a Sun-like Star, *The Astrophysical Journal* **529**, 1, L45–L48, 2000. Publisher: IOP Publishing.

Charbonneau, D., T. M. Brown, R. W. Noyes, and R. L. Gilliland, Detection of an Extrasolar Planet Atmosphere*, *The Astrophysical Journal* **568**, 1, 377, 2002. Publisher: IOP Publishing.

Crossfield, I. J. M., Observations of Exoplanet Atmospheres, *Publications of the Astronomical Society of the Pacific* **127**, 956, 941–960, 2015. Publisher: IOP Publishing.

Deming, D., S. Seager, L. J. Richardson, and J. Harrington, Infrared radiation from an extrasolar planet, *Nature* **434**, 7034, 740–743, 2005. Number: 7034 Publisher: Nature Publishing Group.

Deming, D., A. Wilkins, P. McCullough, A. Burrows, J. J. Fortney, E. Agol, I. Dobbs-Dixon, N. Madhusudhan, N. Crouzet, J.-M. Desert, R. L. Gilliland, K. Haynes, H. A. Knutson, M. Line, Z. Magic, A. M. Mandell, S. Ranjan, D. Charbonneau, M. Clampin, S. Seager, and A. P. Showman, Infrared Transmission Spectroscopy of the Exoplanets HD 209458b and XO-1b Using the Wide Field Camera-3 on the Hubble Space Telescope, *The Astrophysical Journal* **774**, 2, 95, 2013. Publisher: IOP Publishing.

Doyon, R., J. B. Hutchings, M. Beaulieu, L. Albert, D. Lafrenière, C. Willott, D. Touahri, N. Rowlands, M. Maszkiewicz, A. W. Fullerton, K. Volk, A. R. Martel, P. Chayer, A. Sivaramakrishnan, R. Abraham, L. Ferrarese, R. Jayawardhana, D. Johnstone, M. Meyer, J. L. Pipher, and

M. Sawicki, The JWST Fine Guidance Sensor (FGS) and Near-Infrared Imager and Slitless Spectrograph (NIRISS), in *Space Telescopes and Instrumentation 2012: Optical, Infrared, and Millimeter Wave*, vol. 8442, p. 84422R, International Society for Optics and Photonics, 2012.

Ferruit, P., G. Bagnasco, R. Barho, S. Birkmann, T. Böker, G. D. Marchi, B. Dorner, R. Ehrenwinkler, M. Falcolini, G. Giardino, X. Gnata, K. Honnen, P. Jakobsen, P. Jensen, M. Kolm, H.-U. Maier, R. Maurer, M. Melf, P. Mosner, P. Rumler, J.-C. Salvignol, M. Sirianni, P. Strada, M. t. Plate, and T. Wettemann, The JWST near-infrared spectrograph NIRSpec: status, in *Space Telescopes and Instrumentation 2012: Optical, Infrared, and Millimeter Wave*, vol. 8442, p. 84422O, International Society for Optics and Photonics, 2012.

Greene, T. P., M. R. Line, C. Montero, J. J. Fortney, J. Lustig-Yaeger, and K. Luther, CHARACTERIZING TRANSITING EXOPLANET ATMOSPHERES WITHJWST, *The Astrophysical Journal* **817**, 1, 17, 2016. Publisher: American Astronomical Society.

Harrington, J., B. M. Hansen, S. H. Luszcz, S. Seager, D. Deming, K. Menou, J. Y.-K. Cho, and L. J. Richardson, The Phase-Dependent Infrared Brightness of the Extrasolar Planet ω Andromedae b, *Science* **314**, 5799, 623–626, 2006. Publisher: American Association for the Advancement of Science Section: Report.

Kendrew, S., S. Scheithauer, P. Bouchet, J. Amiaux, R. Azzollini, J. Bouwman, C. H. Chen, D. Dubreuil, S. Fischer, A. Glasse, T. P. Greene, P.-O. Lagage, F. Lahuis, S. Ronayette, D. Wright, and G. S. Wright, The Mid-Infrared Instrument for the James Webb Space Telescope, IV: The Low-Resolution Spectrometer, *Publications of the Astronomical Society of the Pacific* **127**, 953, 623, 2015. Publisher: IOP Publishing.

Louie, D. R., D. Deming, L. Albert, L. G. Bouma, J. Bean, and M. Lopez-Morales, Simulated-JWST/NIRISS Transit Spectroscopy of Anticipated Tess Planets Compared to Select Discover-

ies from Space-based and Ground-based Surveys, *Publications of the Astronomical Society of the Pacific* **130**, 986, 044,401, 2018. Publisher: IOP Publishing.

Lovis, C. and D. Fischer, Radial velocity techniques for exoplanets, *Exoplanets* pp. 27–53, 2010. Publisher: University of Arizona Press.

Madhusudhan, N., Exoplanetary Atmospheres: Key Insights, Challenges and Prospects, *Annual Review of Astronomy and Astrophysics* **57**, 1, 617–663, 2019. ArXiv: 1904.03190.

Mandel, K. and E. Agol, Analytic Light Curves for Planetary Transit Searches, *The Astrophysical Journal Letters* **580**, L171–L175, 2002.

Mayor, M. and D. Queloz, A Jupiter-mass companion to a solar-type star, *Nature* **378**, 6555, 355–359, 1995. Number: 6555 Publisher: Nature Publishing Group.

Mayor, M., C. Lovis, and N. C. Santos, Doppler spectroscopy as a path to the detection of Earth-like planets, *Nature* **513**, 7518, 328–335, 2014. Number: 7518 Publisher: Nature Publishing Group.

Mazeh, T., D. Naef, G. Torres, D. W. Latham, M. Mayor, J.-L. Beuzit, T. M. Brown, L. Buchhave, M. Burnet, B. W. Carney, D. Charbonneau, G. A. Drukier, J. B. Laird, F. Pepe, C. Perrier, D. Queloz, N. C. Santos, J.-P. Sivan, S. Udry, and S. Zucker, The Spectroscopic Orbit of the Planetary Companion Transiting HD 209458*, *The Astrophysical Journal Letters* **532**, 1, L55, 2000. Publisher: IOP Publishing.

Perrin, M. D., A. Sivaramakrishnan, C.-P. Lajoie, E. Elliott, L. Pueyo, S. Ravindranath, and L. Albert, Updated point spread function simulations for JWST with WebbPSF **9143**, 91,433X, 2014. Conference Name: Space Telescopes and Instrumentation 2014: Optical, Infrared, and Millimeter Wave.

Pontoppidan, K. M., T. E. Pickering, V. G. Laidler, K. Gilbert, C. D. Sontag, C. Slocum, M. J. S. Jr, C. Hanley, N. M. Earl, L. Pueyo, S. Ravindranath, D. M. Karakla, M. Robberto, A. Noriega-Crespo, and E. A. Barker, Pandeia: a multi-mission exposure time calculator for JWST and WFIRST, in *Observatory Operations: Strategies, Processes, and Systems VI*, vol. 9910, p. 991016, International Society for Optics and Photonics, 2016.

Rein, H., A proposal for community driven and decentralized astronomical databases and the Open Exoplanet Catalogue, *arXiv:1211.7121 [astro-ph, physics:physics]* , 2012. ArXiv: 1211.7121.

Rieke, G. H., G. S. Wright, T. Böker, J. Bouwman, L. Colina, A. Glasse, K. D. Gordon, T. P. Greene, M. Güdel, T. Henning, K. Justtanont, P.-O. Lagage, M. E. Meixner, H.-U. Nørgaard-Nielsen, T. P. Ray, M. E. Ressler, E. F. v. Dishoeck, and C. Waelkens, The Mid-Infrared Instrument for the James Webb Space Telescope, I: Introduction, *Publications of the Astronomical Society of the Pacific* **127**, 953, 584, 2015. Publisher: IOP Publishing.

Sarkar, S., A. Papageorgiou, and E. Pascale, Exploring the potential of the ExoSim simulator for transit spectroscopy noise estimation, in *Space Telescopes and Instrumentation 2016: Optical, Infrared, and Millimeter Wave*, vol. 9904, p. 99043R, International Society for Optics and Photonics, 2016.

Sarkar, S., N. Madhusudhan, and A. Papageorgiou, JexoSim: a time-domain simulator of exoplanet transit spectroscopy with JWST, *Monthly Notices of the Royal Astronomical Society* **491**, 1, 378–397, 2020a. Publisher: Oxford Academic.

Sarkar, S., E. Pascale, A. Papageorgiou, L. J. Johnson, and I. Waldmann, ExoSim: the Exoplanet Observation Simulator, *arXiv:2002.03739 [astro-ph]* , 2020b. ArXiv: 2002.03739.

Seager, S. and D. Deming, Exoplanet Atmospheres, *Annual Review of Astronomy and Astrophysics* **48**, 1, 631–672, 2010.

Seager, S. and D. D. Sasselov, Theoretical Transmission Spectra during Extrasolar Giant Planet Transits, *The Astrophysical Journal* **537**, 916–921, 2000.

Sing, D. K., F. Pont, S. Aigrain, D. Charbonneau, J.-M. Désert, N. Gibson, R. Gilliland, W. Hayek, G. Henry, H. Knutson, A. L. des Etangs, T. Mazeh, and A. Shporer, Hubble Space Telescope transmission spectroscopy of the exoplanet HD 189733b: high-altitude atmospheric haze in the optical and near-ultraviolet with STIS, *Monthly Notices of the Royal Astronomical Society* **416**, 2, 1443–1455, 2011. Publisher: Oxford Academic.

Stevenson, K. B., N. K. Lewis, J. L. Bean, C. Beichman, J. Fraine, B. M. Kilpatrick, J. E. Krick, J. D. Lothringer, A. M. Mandell, J. A. Valenti, E. Agol, D. Angerhausen, J. K. Barstow, S. M. Birkmann, A. Burrows, D. Charbonneau, N. B. Cowan, N. Crouzet, P. E. Cubillos, S. M. Curry, P. A. Dalba, J. de Wit, D. Deming, J.-M. Désert, R. Doyon, D. Dragomir, D. Ehrenreich, J. J. Fortney, A. Garc´a Muñoz, N. P. Gibson, J. E. Gizis, T. P. Greene, J. Harrington, K. Heng, T. Kataria, E. M.-R. Kempton, H. Knutson, L. Kreidberg, D. Lafrenière, P.-O. Lagage, M. R. Line, M. Lopez-Morales, N. Madhusudhan, C. V. Morley, M. Rocchetto, E. Schlawin, E. L. Shkolnik, A. Shporer, D. K. Sing, K. O. Todorov, G. S. Tucker, and H. R. Wakeford, Transiting Exoplanet Studies and Community Targets for *JWST* 's Early Release Science Program, *Publications of the Astronomical Society of the Pacific* **128**, 967, 094,401, 2016.

Wells, M., J.-W. Pel, A. Glasse, G. S. Wright, G. Aitink-Kroes, R. Azzollini, S. Beard, B. R. Brandl, A. Gallie, V. C. Geers, A. M. Glauser, P. Hastings, T. Henning, R. Jager, K. Justtanont, B. Kruizinga, F. Lahuis, D. Lee, I. Martinez-Delgado, J. R. Martinez-Galarza, M. Meijers, J. E. Morrison, F. Müller, T. Nakos, B. O'Sullivan, A. Oudenhuysen, P. Parr-Burman, E. Pauwels, R.-R. Rohloff, E. Schmalzl, J. Sykes, M. P. Thelen, E. F. v. Dishoeck, B. Vandenbussche, L. B. Venema, H. Visser, L. B. F. M. Waters, and D. Wright, The Mid-Infrared Instrument for the James Webb Space Telescope, VI: The Medium Resolution Spectrometer, *Publications of the Astronomical Society of the Pacific* **127**, 953, 646, 2015. Publisher: IOP Publishing.